Journal of Ovonic Research Vol. 9, No. 5, September - October 2013, p. 147 - 155

NUMERICAL ANALYSIS OF PHOTONIC CRYSTAL WAVEGUIDE

D. SAVASTRU, R. SAVASTRU, S. MICLOŞ, I. LANCRANJAN*
National Institute of R&D for Optoelectronics - INOE 2000, 409 Atomistilor St., Magurele, Ilfov, RO-077125, Romania

During the last decade, a major research interest is focused on optical sensors for chemical and biosensing application relaying on refractive index (RI) measurements. Among this class of optical sensors the waveguides confined inside of photonic crystals are of high interest. The application of such RI optical sensors is interesting for both gaseous and aqueous samples and includes measurement of parameters like temperature, humidity, chemical composition and biosensing. The improvement of designing RI optical sensors implies analysis of electromagnetic wave propagation into photonic crystals which is strongly influenced by the internal geometry and by the materials of the photonic crystals. Electromagnetic wave propagation into a 2D photonic crystal consisting of an array of circular or elliptical pillars made of dielectric materials placed into air or water is investigated. Some pillars are removed to make a waveguide with a 90° bend. The laser wavelengths of 632.8, 1064 and 1554 nm are considered. The pillars of the photonic crystal are made of GaAs, GaP or GLS. The electromagnetic wave propagation is analysed using the FEM and perfectly matched layers have been employed as boundary conditions. Comprehensive numerical calculations have been performed considering several transverse dimensions circular or elliptical pillar geometries.

(Received August 11, 2013; Accepted October 03, 2013)

Keywords: Photonic crystal, Waveguides, Nanopillars

1. Introduction

In the last decades, optical sensor based on refractive index (RI) measurements have been extensively investigated being a subject to research interest [1,2]. The application of RI sensors is interesting for both gaseous and aqueous samples and includes measurement of parameters like temperature, humidity, chemical composition and biosensing [1-6]. The application of RI sensors for biosensing has especially gained a high degree of interest within the last period decades. It includes detection of DNA, proteins, antibody-antigen interactions, cells and bacteria. The trend for biosensing systems, when considering the commercial market, aims at specific and label-free detection in various complex media to ease the operation of the sensor. In addition, the sensor elements should preferably be cheap in fabrication, the system should be operated without any moving parts, and the sensitivity should be in the picomolar regime [3,7].

In this regard quite a few commercial sensor systems have also emerged [1-7], where especially the Surface Plasmon Resonance (SPR) sensor and the conventional waveguide sensor are well established and well known technologies. A wide range of photonic crystal (PC) sensing devices has been presented in the literature. Photonic crystal fibre (PCF) is one class of PC devices that has been demonstrated for RI measurements and biosensing [8-11]. However these are difficult to implement in a compact, automated system and the fabrication of PCF sensors is rather tedious. The biosensing techniques relying on the use of PCF's includes detection of fluorescently labelled objects like DNA [10] and specific antibody detection [11]. Sensors based on planar bulk PCs have also been presented for sensing and biosensing in particular [13-15].

* Corresponding author: j_j_f_l@yahoo.com

Components based on planar PCs, also referred to as planar Photonic Crystal Waveguide (PCW) components, where the light is guided along defects such as missing rows of dielectric pillar constituents of PC can be designed to obtain a very high and spatially selective sensitivity to changes in the RI of the surroundings, superior to the planar bulk devices. It is worth to underline that the design of planar PCW components has numerical simulation of electromagnetic wave propagation along PC defects such as missing rows as the main issue.

When analysing the numerical simulation of electromagnetic wave propagation along PC defects it is to be noticed that the PC concept originated in the early 1990s [19, 20] and firstly these structures are foreseen to be important building blocks in future optoelectronic communication networks. In the beginning, the PC were intended for controlling spontaneous emission in optical semiconductor components by exploiting extraordinary properties of periodic structures [21].

The sensing properties of PCW have already been exploited for different simple parameters. Recent applications of PCW include nanofluidic tuning, RI measurements, and optical characterization of molecule orientation [18], however, they have not yet been used for biosensing. Thus, one interesting field of application for PCW components is for biosensing purposes. PCWs can be realized on SOI wafers and have the advantages compared to both conventional evanescent biosensors [12,15,17], PCFs and planar, bulk PC biosensors that they can be made ultra-compact, and integrated with both additional optical and electronic components onto one single chip.

The PCW has a large sensing range making it applicable within a broad dynamic range of RI measurements extending from air to high viscous fluids like oil and it is operated without any rotation of the included parts.

One important problem which appears during the PCW design consists of how to decide the optimum combination of PC pillars semiconductor material in conjunction with electromagnetic wave propagation medium for a measuring system. Also, to some extent, the internal geometry of PCW and of the semiconductor pillar plays appears as important. The main purpose of this paper is to present the first stage results obtained by numerical simulation of electromagnetic wave propagation through a PCW which is built of pillars of different semiconductor material and having different geometry.

2. Theory

The PC concept originated in the early 1990s [19,20] and these structures are foreseen to be important building blocks in future optoelectronic communication networks.

In the beginning, the PC were intended for controlling spontaneous emission in optical semi-conductor components by exploiting extraordinary properties of periodic structures [21]. Unfortunately, the practical realization of PC structures in optics was strongly hampered by a number of obstacles. Among these, the lack of fast and reliable 3D numerical tools, which are able to cope with fully vector Maxwell equations, was a major limitation. The global problem of known numerical recipes was their unstable behaviour in a system that includes regions with large difference in their dielectric constant. Needless to say, the requirements for modelling the PCs are therefore based on the stability properties of the numerical techniques, when handling such abrupt discontinues in the inhomogeneous space function $\varepsilon(r)$. One way of overcoming the discontinuities is to increase the spatial resolution of the system, e.g. to increase the number of grid points associated with the characteristic length of the structure. The characteristic length of the PC is the lattice constant Λ of the periodical pattern. However, increasing the spatial resolution heavily increases the complexity of the computation as the needed computation resources for most of the methods well known in physics and applied in early era of the PC modelling scaled nonlinearly with the growing size of the system.

In band diagram calculations of perfect PCs there is no need to simulate the complete system. It is sufficient to exploit the translation symmetry of the PC. Thus, only a unit cell of lattice structure must be simulated. When, in turn, the concept of the PCW appeared, it led to the super-cell approach, which could be applied in the computation of planar PCW structures by choosing the super-cell correctly and avoiding any coupling between neighbouring super-cells.

However, full 3D simulations of transmission and reflection were still beyond the range of the existing techniques.

Fortunately, researchers turned to the finite-difference time-domain (FDTD) scheme, known in electromagnetics [22]. Attempts to apply this scheme in the modelling of PCs were rather successful. Meanwhile, special absorbing boundary conditions, so called perfectly matched layers (PMLs), had been developed that very effectively terminate numerical volumes in 2D and 3D leading to only very small back reflections. The FDTD method implemented with PMLs has recently been widely accepted as a very powerful computational technique in the modelling of PCs. The complexity of the FDTD method scales only linearly with time and space. Thus, the FDTD scheme is favoured compared to most other numerical methods for PC simulations.

However, the FDTD scheme is very demanding in terms of memory and speed of the available computer hardware when applied to practical 3D problems such as analysis of transmission spectra of PCW in layered structures with 2D patterning. The method does not take full advantage of the periodicity, unlike what is the case in most band diagram calculations. The use of symmetry conditions may only reduce the required memory resources by a factor of four for straight PCWs. Other passive system elements, such as Y-splitters, zigzags-bends, and vertical couplers have even less symmetry.

The application of FDTD codes to various problems in PCW design has recently been demonstrated in Refs. [23–35]. Some of the papers [24,27,28-31,35] address the modelling of transmission spectra in 3D that is essential for studying the features of realistic PCWs. This applies in particular to the losses of the PCW modes [27], which do not appear in 2D calculations. A defect mode in the band gap of a 2D photonic crystal propagates without loss.

However, propagation of the defect modes in a 3D system requires basic restrictions of total-internal-reflection to be fulfilled to avoid out-of-plane propagation.

Most of the existing FDTD codes are able to produce qualitatively correct transmission spectra when compared to experimental data. However, frequency discrepancies around 5-10 % or more are often observed, and empirical parameters are in some cases introduced to get better agreement. In this paper comprehensive FDTD calculations are reported employing PML boundary conditions. Special care is taken in the border regions where two or three PMLs overlap. An advantageous consequence of this analytical approach is that it only is necessary to update the E and H fields during the calculations. In addition, a simple spatial representation is utilized allowing the fields in the PMLs and the main region, respectively, to be treated similarly in the calculation cycles. Thereby, the same internal organization of the calculations is ensured everywhere in the modelled structure. We find that FDTD code produces quantitatively accurate results.

Nevertheless, all the above theoretical considerations can be reduced to a more practical procedure, point of view, by observing the fact that the performed simulations point to study TE waves propagating through the crystal. To model these, it is use a scalar equation for the transverse electric field component E_z,

$$-\nabla \cdot \nabla E_z - n^2 k_0^2 E_z = 0$$

where n is the refractive index and k_0 is the free-space wave number. This simple but still implying large amount of computer calculations numerical procedure is used in the frame of INOE Thin Films Deposition Facility for designing purpose [39-41].

3. Results

The numerical simulation is performed on an array of 10×10 semiconductor pillars as presented in Fig. 1. The semiconductor pillars are considered to be made of GaAs, GaP or GLS. The vertical or horizontal distance, d, between the rows is set to 375 nm. Several cross section geometries of the semiconductor pillars were considered, but, for technological reasons, imposed by the ease of fabrication, square and rectangular pillar cross-sections were abandoned. Circular and elliptical cross-section geometry was intensively investigated. The investigated ellipse large

semi-axes were 70 nm, 100 nm and 140 nm, all with a 35 nm small semi-axis. In the case of elliptical cross-section pillar, the ellipse large axis can be inclined at 0˚, 45˚, 90˚ and 135˚ versus the positive x-axis. In Fig. 1, the 90˚ bent light waveguide formed by a missing row of pillars can be observed.

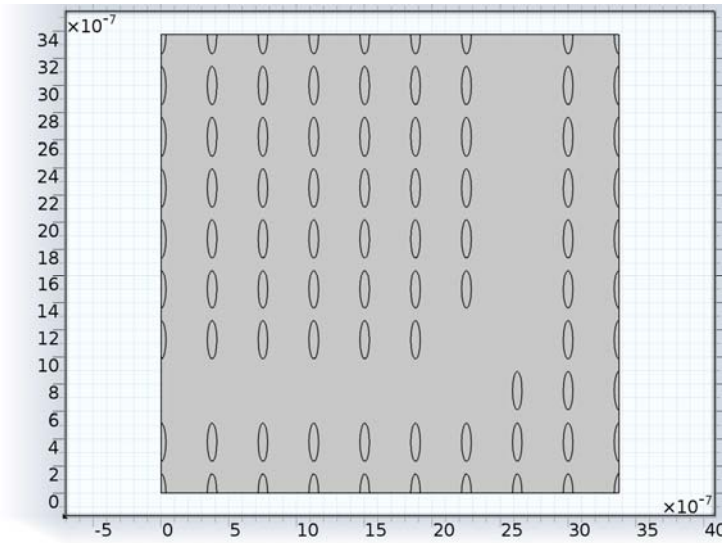

Fig. 1. The geometry of the Photonic Crystal Waveguide.

In Fig. 2 an example of discretization applied on the PCW is presented. The characteristic dimension of the discretization is of 10^{-9} m, being up to three orders of magnitude smaller compared to the laser wavelengths (632.8 nm - He-Ne and diode lasers, 1064 nm - Neodymium lasers and 1554 nm - Erbium lasers) and up to two orders of magnitude smaller than the PC pillar dimensions. The discretization grid can be considered as appropriate for the proposed simulation task.

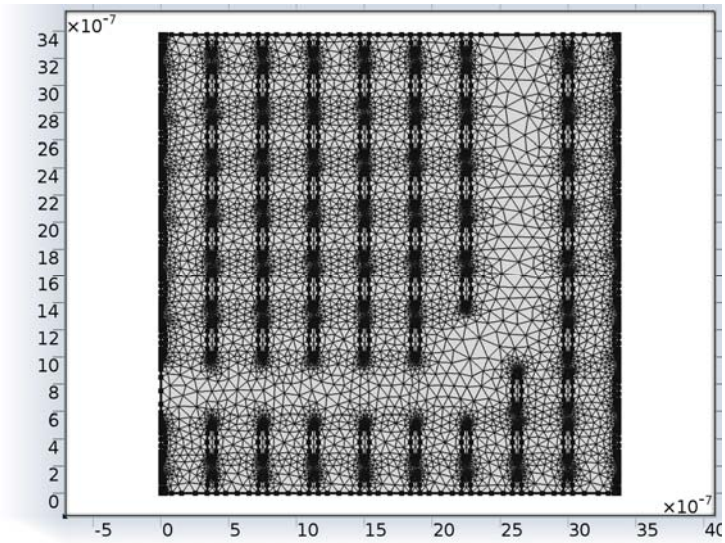

Fig. 2 - Typical discretization of the Photonic Crystal Waveguide.

The distribution transverse electric field z component in the entire PCW structure is obtained. In Fig. 3 is presented the simulation result obtained in the case of PCW made of 140 nm main axis GaAs pillars inclined by 135˚ from the positive x-axis.

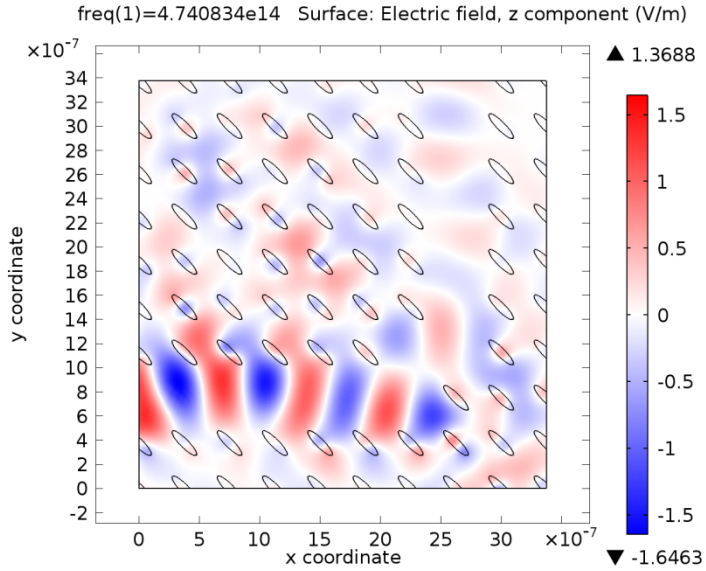

Fig. 3 - The distribution of the transverse electric field z component simulated in the case of PCW made of 140 nm main axis GaAs pillars inclined by 135˚ from the positive x-axis.

The performed simulations have a common task: to define the transverse electric distribution along the horizontal segment of the 90˚ bent waveguide. It is noteworthy that the transverse electric distribution can be simulated along other cut lines considered as interesting. The presented simulation results are obtained considering air as the electromagnetic wave propagation medium.

In Fig. 4, 5 and 6 are presented such results obtained in the case of a PCW made of GaAs 70×35 nm, 100×35 nm and 140×35 nm elliptic pillars inclined by 0˚, 45˚, 90˚ and 135˚ from the positive x-axis. In Fig. 7, 8 and 9 present the results obtained in the case of a PCW made of GaP 70×35 nm, 100×35 nm and 140×35 nm elliptic pillars inclined by 0˚, 45˚, 90˚ and 135˚ from the positive x-axis. Finally Fig. 10, 11 and 12 present the results obtained in the case of a PCW made of GLS 70×35 nm, 100×35 nm and 140×35 nm elliptic pillars inclined by 0˚, 45˚, 90˚ and 135˚ from the positive x-axis. In the legend some notations were made: A means 70x35 nm ellipse, B – 100x35 nm ellipse and C - 140x35 nm ellipse, while E0, E45, E90 and E135 means ellipse inclined by 0, 45, 90 or 135°.

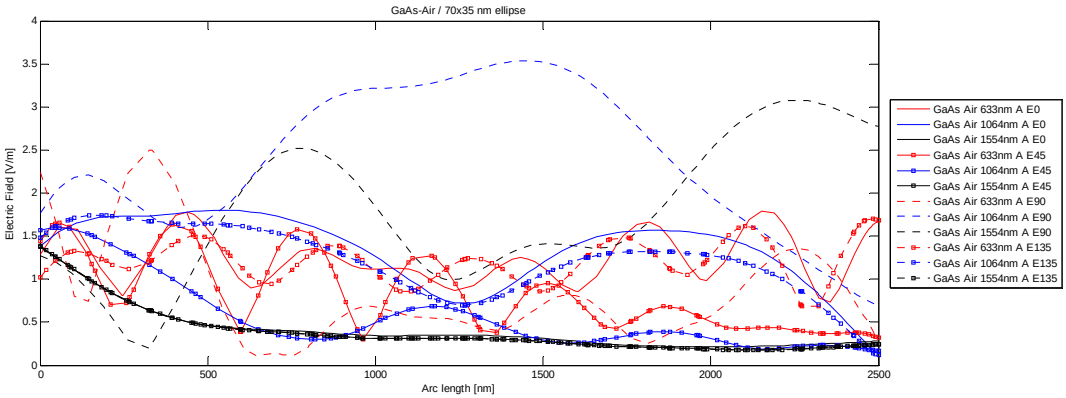

Fig. 4 – Study of GaAs-Air, 70 x 35 nm ellipses.

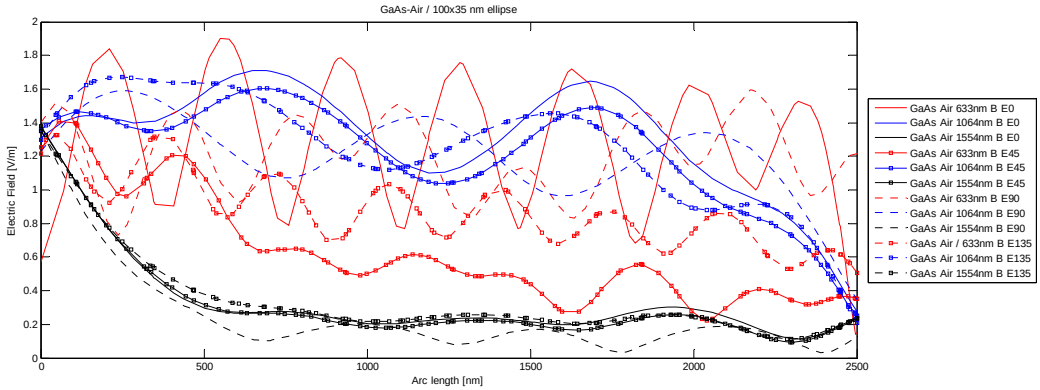

Fig. 5 – Study of GaAs-Air, 100 x 35 nm ellipses.

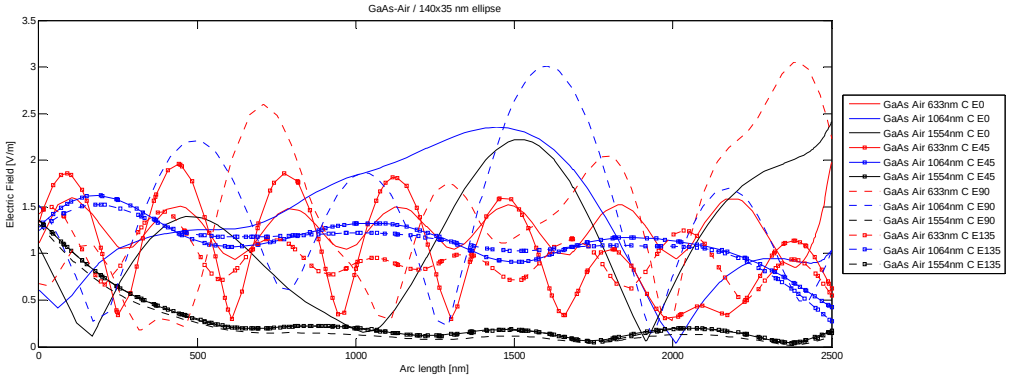

Fig. 6 – Study of GaAs-Air, 140 x 35 nm ellipses.

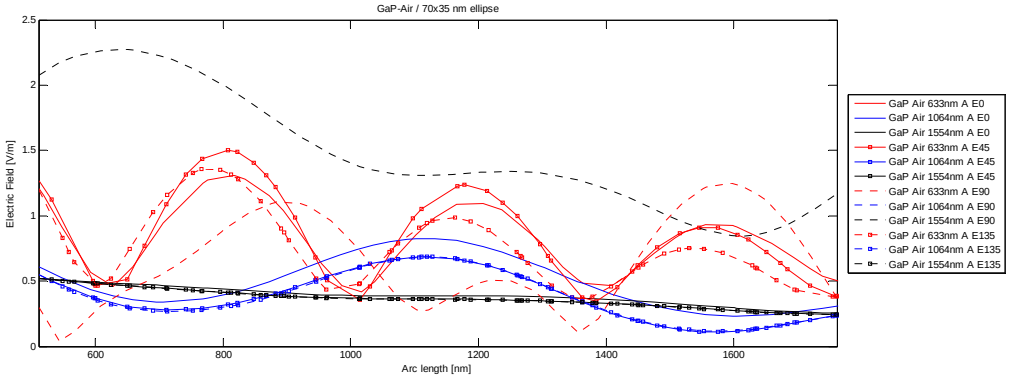

Fig. 7 – Study of GaP-Air, 70 x 35 nm ellipses.

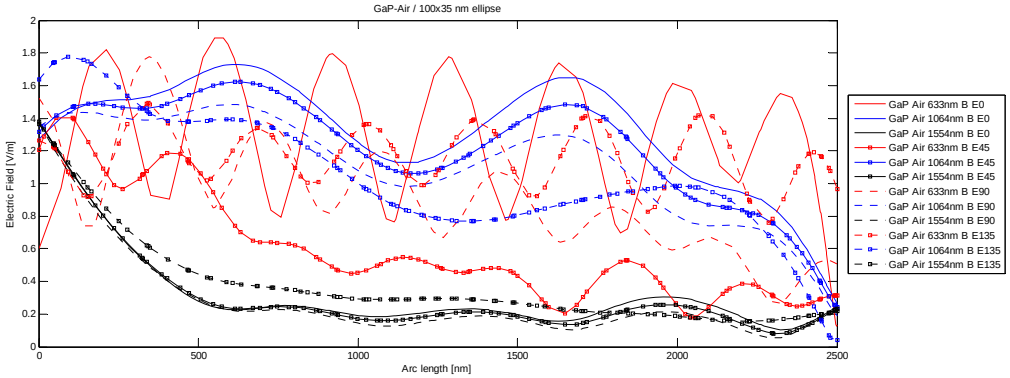

Fig. 8 – Study of GaP-Air, 100 x 35 nm ellipses.

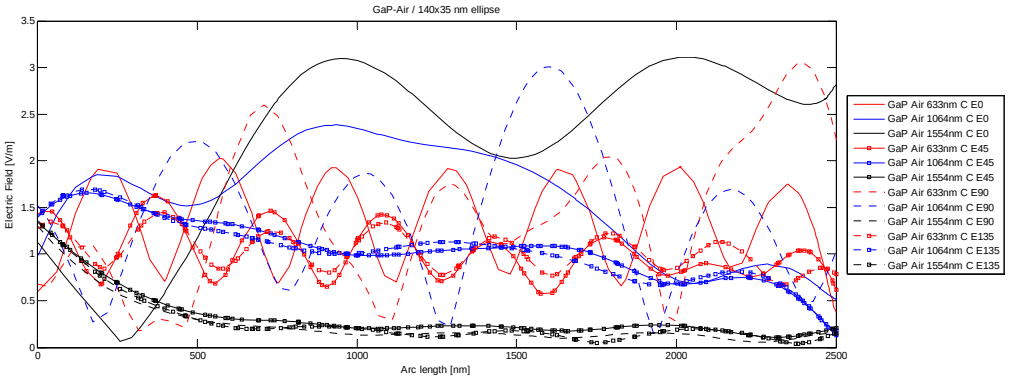

Fig. 9 – Study of GaP-Air, 140 x 35 nm ellipses.

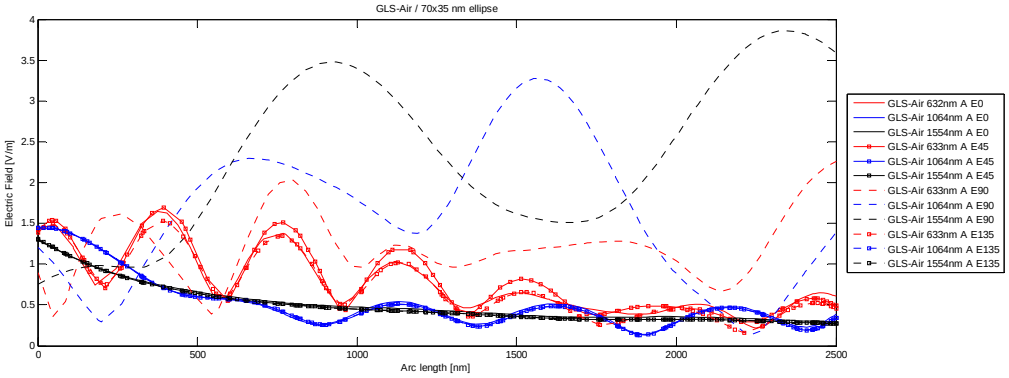

Fig. 10 – Study of GLS-Air, 70 x 35 nm ellipses.

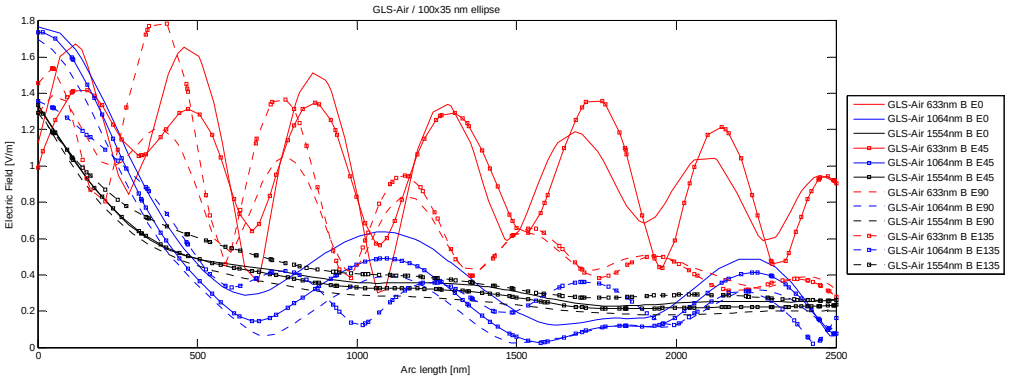

Fig. 11 – Study of GLS-Air, 100 x 35 nm ellipses.

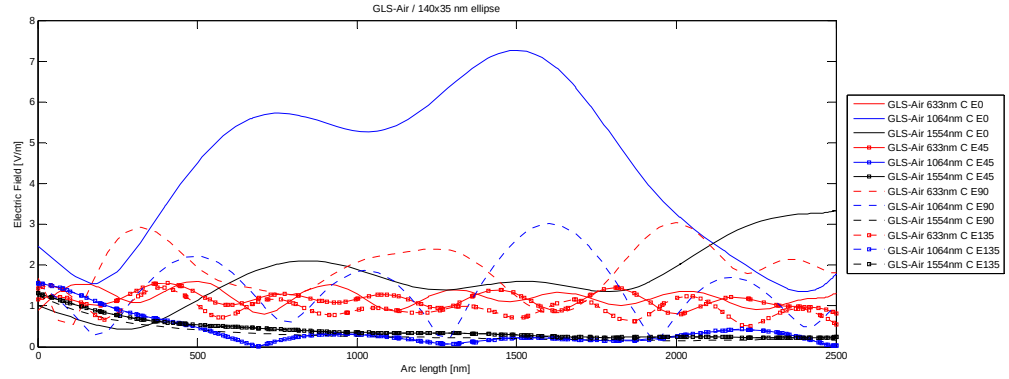

Fig. 12 – Study of GLS-Air, 140 x 35 nm ellipses.

4. Discussion and conclusions

A first glance analysis of the simulation results implies several observations to be made:

- The transverse electric z component distribution along the horizontal segment of the 90˚ bent waveguide indicates an improved propagation along PCW for larger contrast material, i.e. for semiconductor material with the large refraction index in comparison to the air, such as GaAs. This effect is more important in the case of GaAs and less accentuated for GaP.
- The electric field with 632.8 nm wavelength propagates over longer distances inside PCW.
- With several exceptions, the longer wavelengths electric fields, 1554 nm and 1064 nm, inside PCW, have decay with stronger factor compared to 632.8 nm wavelength.
- The Electric Field values depend on the pillar ellipse inclination angle, being larger for 45˚ and 90˚ angles.
- There is an exception at the preceding observation - the largest Electric Field value (~7 V/m) is observed in the case of 1064 nm wavelength incident on GLS made PCW in which the pillar ellipse is not inclined.
- The largest difference between the Electric Field values observed in the cases of transmitted and absorbed along the waveguide investigated horizontal portion is observed for GLS 140×35 nm made PCW with 0˚ inclination.

The above mentioned results provide us with a tool of choosing materials, wavelength and pillars geometry when designing a PCW sensor.

As propagation medium was chosen the air, but only as a first step and calibration of the method. A second step is to replace air by another medium (gas or liquid) and study the effect of small changes in the medium refractive index, to measure thus the sensitivity of the sensor.

The main purpose of the paper consists in presenting first glance results obtained using a simulation methodology applied in the case of PCW design performed at INOE. The presented results appear as promising mainly in respect of further developments including the role of electromagnetic wave propagation medium.

Acknowledgements

The presented results were obtained in the frame of Romanian National Authority for Scientific Research PARTNERSHIP in PRIORITY DOMAINS PROGRAMME Contract nr 25/2012 – "2D Plasmonic Optical Memory with active calchogenide glass layer" – MEMOPLAS.

References

[1] B. Sepulveda, A. Calle, L.M. Lechuga, G. Armelles, Opt. Lett. **31**, 1085 (2006).
[2] N. Skivesen, A. Tetu, M. Kristensen, J. Kjems, Opt. Express **15**, 3169 (2007).
[3] G.A. Robinson, Biosens. Bioelectron. **6**,183 (1991).
[4] C. Nylander, B. Liedberg, T. Lind, Sens.Actuators **3**, 79 (1982).
[5] J. Homola, S.S. Yee, G. Gauglitz, Sens. Acuators B **54**, 3 (1999).
[6] J.S. Yuk, S. Yi, H.G. Lee, H.J. Lee, Y. Kim, K. Ha, Sens. Actuators B **94**, 161 (2003).
[7] F. Hook, J. Vorors, M. Rodahl, R. Kurrat, P. Boni, J.J. Ramsden, M. Textor, N.D. Spencer, P. Tengvall, J. Gold, B. Kasemo, Colloids and surfaces, B **24**, 155 (2002).
[8] R. Kurrat, B. Walivaara, A. Marti, M. Textor, P. Tengvall, J.J. Ramsden, N.D. Spencer, Colloids and Surfaces, B **11**, 187 (1998).
[9] J.M. Fini, Meas. Sci. Technol. **15**, 1120 (2004).
[10] J.B. Jensen, L.H. Pedersen, P.E. Hoiby, L.B. Nielsen, J.R. Folkenberg, J. Riishede, D. Noordegraaf, K.Nielsen, A. Carlsen, and A. Bjarklev, Opt. Lett. **29**, 1974 (2004).
[11] J.B. Jensen, P.E. Hoiby, G. Emiliyanov, O. Bang, L.H. Pedersen, A. Bjarklev, Opt. Express **13**, 5883 (2005).
[12] E. Chow, A. Grot, L.W. Mirkarimi, M. Sigalas, G. Girolami, Opt. Lett. **29**, 1093 (2003).

[13] L.W. Mirkarimi, S. Zlatanovic, M.S. Sigalas, M.A. Bynum, K. Robotti, E. Chow, A. Grot, LEOS summer topical meetings, Quebec, Canada (2006).
[14] W. Bogaerts, V. Wiaux, D. Taillaert, S. Beckx, R. Baets, Proceedings of SPIE (2003).
[15] B. Cunningham, P. Li, B. Lin, J. Pepper, Sens. Actuators B **81**, 316 (2002).
[16] L.L. Chan, B.T. Cunningham, P.Y. Li, D. Puff, Sens. Actuators B **120**, 392 (2007).
[17] O.Levi, W. Suh, M.M. Lee, J. Zhang, S.r.J. Brueck, S. Fan, J.S. Harris, CLEO/QELS Technical Conference, Long Beach, USA, 23 May 2006.
[18] J. Topolancik, P. Bhattacharya, J. Sabarinathan, P.C. Yu, Appl. Phys. Lett. **82**, 1143 (2003).
[19] S. John, Phys. Rev. Lett. **58**, 2486 (1987).
[20] E. Yablonovitch, Phys. Rev. Lett. **58**, 2059 (1987).
[21] V. P. Bykov, Radiation of atom in a resonant environment, World Scientific, Singapore, 1993.
[22] A.Taflove, S. C. Hagness, Computational electrodynamics: The finite-difference time-domain method, Artech House, Boston, 2000.
[23] S. Fan, Appl. Phys. Lett. **80**, 908 (2002).
[24] Y. Sugimoto et al., J. Appl. Phys. **91**, 922 (2002).
[25] K. Yamada et al., Opt. Commun. **198**, 395 (2001).
[26] M. Loncar et al., J. Opt. Soc. Am. B **9**, 1362 (2001).
[27] M. Agio, C. M. Soukoulis, Phys. Rev. E **64**, 055603 (2001).
[28] T. Ochiai, K. Sakoda, Phys. Rev. B **63**, 125107 (2001).
[29] E. Chow et al., Opt. Lett. **26**, 286 (2001).
[30] A. Chutinan, S. Noda, Phys.Rev. B **62**, 4488 (2000).
[31] A. Adibi et al., J. Lightwave Technol. **18**, 1554 (2000).
[32] M. Qiu, S. He, Phys. Rev. B **61**, 12871 (2000).
[33] Y. Sugimoto, N. Ikeda, N. Carlsson, K. Asakawa, N. Kawai, K. Inoue, IEEE J. Quantum Electron.**38**, 760 (2002).
[34] H. Benisty et al., IEEE J. Quantum Electron. **38**, 770 (2002).
[35] R. Ferrini, D. Leuenberger, M. Mulot, M. Qiu, J. Moosburger, M. Kamp, A. Forchel, S. Anand, R. Houdre, IEEE J. QuantumElectron. **38**, 786 (2002).
[36] J. Ward, J. B. Pendry, Comput. Phys. Commun. 128, 590-621 (2000).
[37] A.J.Ward, J. B. Pendry, J. Mod. Opt. **43**, 773 (1996).
[38] S. D. Gedney, IEEE Trans. Ant. Prop. **44**, 1630 (1996).
[39] I. Lancranjan, S. Miclos, A. Popescu, D. Savastru, I. Mihailescu, ROMOPTO 2012, Sept. 3-6, 2012, Bucharest, Romania
[40] S. Miclos, D. Savastru, I. Lancranjan, R. Savastru, C. Opran, PIERS 2013 in Stockholm, Sweden, 12-15 August, 2013
[41] D. Savastru, R. Savastru, S. Miclos, I. Lancranjan, NCM 12, July 7-12, 2013, Riva del Garda, Italy